Metastable Oxides with Magnetic Functionalities*)

Katsuhisa TANAKA

Graduate School of Engineering, Kyoto University, Kyoto 615-8510, Japan

(Received 29 January 2023 / Accepted 7 July 2023)

Inorganic solid-state materials comprise several types of polymorphs with different structures and properties. Among these, only one of the polymorphs is stable, whereas the others are metastable at ambient temperature and pressure. Sometimes, metastable phases exhibit more curious structures and properties and excellent functionalities than those of the stable phase. Such a phenomenon has been observed in magnetic properties of oxides as well. This paper presents some metastable oxides that manifest magnetic properties and functionalities never observed in their stable counterparts; ferrimagnetism of spinel-type $ZnFe_2O_4$ with high magnetization and a high magnetic-phase transition temperature; ferromagnetism observed in metastable Eu^{2+}-based perovskite-type oxides, such as $EuTiO_3$, $EuZrO_3$, and $EuHfO_3$; and ferromagnetism of the amorphous oxides containing a large amount of Eu^{2+} ions. Amorphous oxides clearly exhibiting ferromagnetic transition are very rare.

Keywords: oxide, metastable phase, magnetic properties, ferromagnetism, ferrimagnetism, zinc ferrite, perovskite, divalent europium, amorphous phase

DOI: 10.1585/pfr.18.2101078

1. Introduction

Magnetic oxides and their properties have gained considerable research attention in fundamental science and practical applications. In particular, ferrites, i.e., compounds based on iron oxides, have been an object of study in solid-state physics and chemistry and have been practically utilized as magnetic materials such as permanent magnet, magnetic core, recording medium, optical isolator, and magnetic fluids [1]. Among the ferrites, magnetite (Fe_3O_4), which is a prototype of ferrimagnetic oxide and has applications in magnetic fluids, drug delivery systems, catalysts, etc., is an ongoing research object in the field of solid-state physics; studies have been conducted to determine its rather complicated electronic structure that is closely related to both electronic conduction and magnetic ordering [2], although the compound, included in the earth's crust, is ubiquitous. Recently, Fe_3O_4 has attracted attention from the point of view of application in spintronics devices because of the high-spin polarizability of conduction electrons. These days, novel phenomena have been discovered in magnetic oxides, such as the spin current and spin Hall effect observed in the $Y_3Fe_5O_{12}$ thin film [3], formation of skyrmion in the interface between $SrRuO_3$ and $SrIrO_3$ [4], magnon Hall effect in $Lu_2V_2O_7$ [5], and multiferroic properties of many transition metal oxides, such as $TbMnO_3$ [6], $LiNiPO_4$ [7], and $CoCr_2O_4$ [8].

In addition to oxide crystals, other inorganic crystalline materials have some polymorphs or allotropes with different structures and properties. A typical example is carbon. As is well known, graphite and diamond are the allotropes of carbon, where graphite is more stable at ambient temperature and pressure, although diamond can exist in its metastable phase even at ambient temperature and pressure. The properties and crystal structures differ between these two allotropes; graphite is black, brittle, and an electrical conductor, whereas diamond is transparent, hard, and is an electrical insulator. In this case, both stable and metastable phases of the crystalline carbon have excellent properties that can be applied practically. However, in some cases, the metastable phase shows functionalities superior to those of its stable counterpart. For example, consider the dielectric properties of HfO_2. The stable phase of HfO_2 possesses a monoclinic structure and is paraelectric, whereas orthorhombic HfO_2, a metastable phase, exhibits ferroelectric properties [9]. Therefore, HfO_2 can be used as a novel memory device [10].

This paper presents some examples of oxides, the magnetic functionalities of the metastable phase of which are superior to those of its stable counterpart. Metastable spinel-type $ZnFe_2O_4$ portrays high magnetization, high Curie temperature, and large Faraday effect in the short-wavelength range. These properties are also displayed during the ferromagnetism of the metastable phases of perovskite-type $EuTiO_3$, $EuZrO_3$, and $EuHfO_3$ as well as amorphous oxides containing a large amount of Eu^{2+} ions. Experimental and theoretical analyses were conducted to discuss the microscopic mechanisms of the magnetic interactions that result in such magnetic functionalities. In general, the metastable solid-state oxide can be derived through a nonequilibrium process from a high-entropy state, such as the gas phase; therefore, the so-called "plasma" is very effective for the preparation of the metastable solid-state phase. For example, plasma-

author's e-mail: tanaka.katsuhisa.4n@kyoto-u.ac.jp

*) This article is based on the presentation at the 31st International Toki Conference on Plasma and Fusion Research (ITC31).

enhanced chemical vapor deposition was applied to the fabrication of oxide thin films. Hence, the development of plasma science and technology is becoming increasingly significant for efficiently obtaining metastable oxides with excellent functionalities.

2. High Magnetization, High Magnetic-Phase Transition Temperature, and Large Faraday Effect of Metastable $ZnFe_2O_4$

The stable phase of $ZnFe_2O_4$ possesses a normal spinel-type structure, in which all Zn^{2+} ions occupy the tetrahedral sites and all Fe^{3+} ions occupy the octahedral sites in the face-centered cubic arrangement of oxide ions. Figure 1 (a) schematically illustrates the crystal structure of the normal spinel-type $ZnFe_2O_4$, in which a negative superexchange interaction is observed between Fe^{3+} ions in the octahedral sites. Therefore, antiferromagnetic configuration of the magnetic moments appears as a stable magnetic phase below the magnetic transition temperature (Néel temperature). In this case, the superexchange interaction is rather weak because the Fe-O-Fe bond angle is 90°, as shown in Fig. 1 (a). Hence, the Néel temperature of normal spinel-type $ZnFe_2O_4$ is as low as 10 K [11, 12].

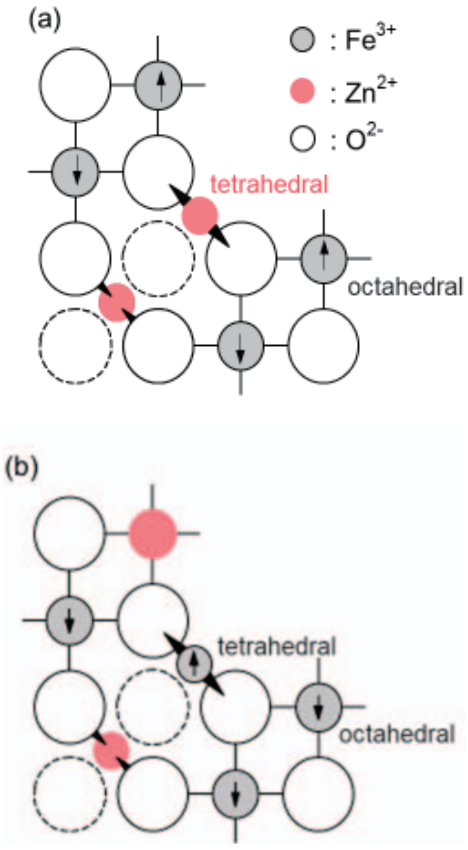

Fig. 1 Schematic of the crystal structure for (a) normal spinel-type and (b) random spinel-type $ZnFe_2O_4$. Note that the random spinel-type $ZnFe_2O_4$ is in its metastable phase.

Suppose that a random distribution of cations, i.e., Zn^{2+} and Fe^{3+} ions, is introduced into the crystal structure, as illustrated in Fig. 1 (b), then the magnetic structure could be drastically changed. In such a random spinel-type structure, Fe^{3+} ions occupy both tetrahedral and octahedral sites, so that the superexchange interaction is dominant between the Fe^{3+} ions in the octahedral and tetrahedral sites. This interaction is rather strong because the Fe-O-Fe bond angle is close to 180°. Although this interaction is negative, ferrimagnetism could be observed because of the difference between the numbers of octahedral and tetrahedral Fe^{3+} ions. Thus, high magnetization and high ferrimagnetic phase-transition temperature, i.e., Curie temperature, are expected for the random spinel-type $ZnFe_2O_4$.

Previous studies have realized the random spinel-type structure of $ZnFe_2O_4$ by rapidly quenching the $ZnFe_2O_4$ melt [13, 14] or by the nonequilibrium condensation from the gas phase. For the latter, a thin film of $ZnFe_2O_4$ was prepared using the sputtering method [15, 16]. Figure 2 shows the magnetic-field dependence of magnetization (so-called M–H curve) at 300 K for as-deposited $ZnFe_2O_4$ thin film on a commercially available Corning 7059 glass substrate. The magnetization rapidly increases with an increase in the magnetic field and can be saturated at rather low magnetic fields. The saturation magnetization is 32 emu/g, which reaches one third of the saturation magnetization of Fe_3O_4, a prototype of ferrimagnetic oxide, as described earlier. The inset in Fig. 2 depicts an enlarged view of the low magnetic-field region of the M–H curve. Although small, this curve manifests a hysteresis loop. These experimental results clearly indicate that the as-deposited $ZnFe_2O_4$ thin film is ferrimagnetic with high magnetization and a Curie temperature higher than room temperature.

Nakashima *et al.* [17] performed X-ray absorption near-edge structure (XANES) spectroscopy and analysis of the Zn K-edge spectra based on the first-principles calculations by using the density functional theory to confirm

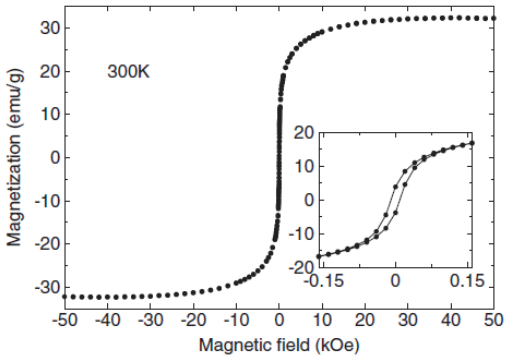

Fig. 2 Magnetization as a function of magnetic field at 300 K for as-deposited thin film prepared using the sputtering method. The inset shows an enlarged view of the low magnetic-field region. Reprinted with permission from Ref. [16].

the random distribution of Zn^{2+} ions. In the study, the experimental XANES spectra of the as-deposited $ZnFe_2O_4$ thin film and those annealed at low temperatures, such as 300 and 400°C, were accurately reproduced by assuming that the spectra comprise the theoretical spectra calculated for tetrahedral and octahedral Zn^{2+} ions. The quantitative analysis leads to the conclusion that the chemical formula for the as-deposited thin film and those annealed at low temperatures is $(Zn_{0.4}Fe_{0.6})_T[Zn_{0.6}Fe_{1.4}]_OO_4$, where subscripts T and O denote the tetrahedral and octahedral sites, respectively. In other words, as much as 60% of Zn^{2+} ions occupy the octahedral sites, indicating that random distribution is achieved in these $ZnFe_2O_4$ thin films.

The present thin films of metastable or random spinel-type $ZnFe_2O_4$ exhibit a large Faraday effect, in particular, in the short-wavelength region [15, 18]. The Faraday effect, a magneto-optical property, is a phenomenon in which a linearly polarized light is converted into an elliptically polarized light by rotating the plane of polarization or the principal axis of the elliptically polarized light with respect to the initial state after the light passes through a magnetic material, provided that the propagation direction of the incident light is parallel to the magnetization or magnetic field. The rotation angle is called Faraday rotation angle and is an important parameter when applying the Faraday effect to devices such as an optical isolator, a magnetic field sensor, and an electric current sensor. Figure 3 shows the dependence of Faraday rotation angle on the wavelength for as-deposited and annealed $ZnFe_2O_4$ thin films. The annealing was conducted at 300, 400, and 800°C in air. As shown in Fig. 3, an intense Faraday rotation angle is observed around 400 nm for the as-deposited thin film and those annealed at 300 and 400°C, while the thin film annealed at 800°C manifests a very small rotation angle. The magnetization measurements demonstrate that the room-temperature magnetization for the thin films annealed at 300 and 400°C is comparable to that of the as-deposited thin film. However, the magnetization is drastically reduced when the annealing temperature is above 600°C [19, 20]. In addition, the Zn-edge XANES spectroscopy confirms that the $ZnFe_2O_4$ thin film obtained through annealing at 800°C achieves the normal spinel-type structure, i.e., all the Zn^{2+} ions occupy the tetrahedral sites. These facts clearly indicate that the random spinel-type structure of metastable $ZnFe_2O_4$ is converted into the normal spinel-type structure of the stable phase when the metastable phase is annealed at higher temperatures. In addition, Fig. 3 reveals that annealing at low temperatures increases the Faraday rotation angle. Similarly, the magnetization is increased by performing annealing at 300 and 400°C. This fact may be explained in terms of the decrease in the number of oxygen vacancies, which could exist in the as-deposited thin film, owing to the nonequilibrium process in which the $ZnFe_2O_4$ thin film is formed from the gas phase, i.e., high-entropy state.

The maximum value of the Faraday rotation angle was

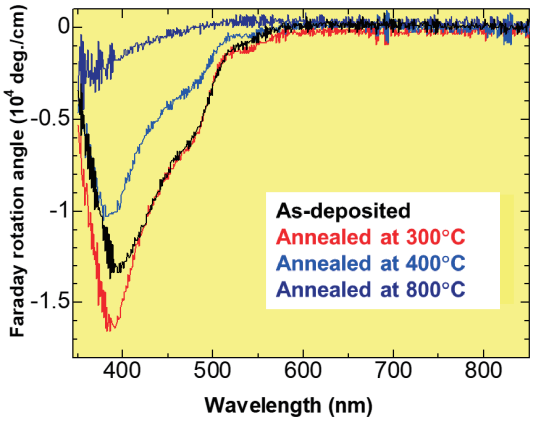

Fig. 3 Wavelength dependence of Faraday rotation angle for as-deposited and annealed thin films of $ZnFe_2O_4$.

observed for the $ZnFe_2O_4$ thin film annealed at 300°C and is 1.65×10^4 °/cm at a wavelength of 386 nm, as shown in Fig. 3. The wavelength of this maximum angle corresponds to the electronic transition related to the Fe^{3+} ions in the ferrimagnetic $ZnFe_2O_4$, as observed for as-deposited and low-temperature-annealed thin films. In contrast, as the thin film of $ZnFe_2O_4$ annealed at 800°C is paramagnetic at room temperature, the magnetization is almost zero and the Faraday rotation is barely observed. The value, 1.65×10^4 °/cm, is comparable to those reported for typical ferrites. For example, the Faraday rotation angle is 3.9×10^4 °/cm for Fe_3O_4 at 632.8 nm [21], 5×10^3 °/cm for $Gd_3Fe_5O_{12}$ at 520 nm [22], 1.2×10^5 °/cm for $Gd_{1.6}Bi_{1.4}Fe_5O_{12}$ at 520 nm [22], and 1.3×10^5 °/cm for $Y_{2.5}Bi_{0.5}Fe_5O_{12}$ at 3.0 eV (410 nm) [23]. Note that garnet-type ferrites, such as $(Y,Bi)_3Fe_5O_{12}$ and $(Gd,Bi)_3Fe_5O_{12}$, have been effectively utilized as optical isolators in optical telecommunications.

3. Ferromagnetism of Metastable Perovskite Oxides Based on Eu^{2+}

Oxides with a perovskite structure are often represented by the formula ABO_3, where the A-site is occupied by a larger cation surrounded by 12 oxide ions and the B-site is an octahedral site occupied by a smaller cation. Group-4 elements, i.e., Ti, Zr, and Hf can compose the perovskite structure with the divalent europium ion to form $EuTiO_3$, $EuZrO_3$, and $EuHfO_3$, respectively. At ambient temperature and pressure, the crystal structure for $EuTiO_3$ is cubic and orthorhombic for $EuZrO_3$ and $EuHfO_3$. $EuTiO_3$ and $EuZrO_3$ have been found to exhibit a magneto-electric effect, and can thus be regarded as multiferroics [24, 25]. In terms of magnetism, the stable phase of these compounds exhibits antiferromagnetic transition at approximately 4 - 5 K [26, 27].

Some theoretical calculations have predicted that the ferromagnetic structure becomes more stable than the antiferromagnetic structure of $EuTiO_3$ when a compressive

strain is induced in the *ab* plane or the lattice volume is increased [28, 29]. These theoretical predictions have been supported by experimental results. Fujita *et al.* [30] prepared an $EuTiO_3$ epitaxial thin film on a $SrTiO_3$ substrate with (001) plane by using the pulsed laser deposition (PLD) method and found that the lattice of the $EuTiO_3$ thin film is elongated along the direction perpendicular to the thin-film surface. They also disclosed that the $EuTiO_3$ thin film with the lattice elongation shows ferromagnetic rather than antiferromagnetic transition at approximately 4 K. Lee *et al.* [31] demonstrated that both ferromagnetism and ferroelectricity are induced in the $EuTiO_3$ thin film when a tensile strain is applied.

Tanaka *et al.* [32] obtained $EuTiO_3$ epitaxial thin films on $LaAlO_3$, $SrTiO_3$, and $DyScO_3$ substrates by using the PLD method. Among these perovskite oxides, the lattice constant is the smallest for $LaAlO_3$ (0.3790 nm) and the largest for $DyScO_3$ (0.3944 nm). In addition, the lattice constants of $SrTiO_3$ and $EuTiO_3$ are almost the same, i.e., 0.3905 nm. They observed that the lattice volume of $EuTiO_3$ is the smallest and the largest for the thin films on $LaAlO_3$ and $DyScO_3$ substrates, respectively. Moreover, all the as-deposited $EuTiO_3$ thin films exhibited ferromagnetic transition, whereas the bulk $EuTiO_3$ is antiferromagnetic. In addition, the magnetization of the $EuTiO_3$ thin films at 2 K was the smallest and largest on $LaAlO_3$ and $DyScO_3$ substrates, respectively. In other words, the ferromagnetism, which was never observed for the stable phase of $EuTiO_3$, was stabilized with the increase in the lattice volume.

Calculations based on the Hybrid Hartree–Fock density functional theory were performed to clarify the mechanism resulting in the stabilization of the ferromagnetic structure of $EuTiO_3$ with an enlarged lattice [33]. The spin Hamiltonian is expressed as follows:

$$H = -2\sum_{i,j} J_{ij}\boldsymbol{S}_i\boldsymbol{S}_j, \quad (1)$$

where $\boldsymbol{S}_i$ and $\boldsymbol{S}_j$ are the spins at the i-th and j-th sites, respectively, and J_{ij} is the exchange coupling constant between the i-th and j-th sites. The energy of different types of magnetic structures, i.e., ferromagnetic, A-type antiferromagnetic, and G-type antiferromagnetic structures, with the arrangement of magnetic moments, as shown in Fig. 4, can be derived as follows:

$$E_F = E_0 + 2S(S+1)(-12J_1 - 24J_2), \quad (2)$$
$$E_A = E_0 + 2S(S+1)(-4J_1 + 8J_2), \quad (3)$$
$$E_G = E_0 + 2S(S+1)(12J_1 - 24J_2), \quad (4)$$

where E_F, E_A, and E_G are the energies of the ferromagnetic, A-type antiferromagnetic, and G-type antiferromagnetic structures, respectively. Further, J_1 and J_2 are the exchange coupling constants for the nearest-neighboring and next-nearest-neighboring magnetic moments, respectively. Figure 5 (a) depicts the lattice volume dependence of energy difference, E_A–E_G and E_F–E_G. When the change

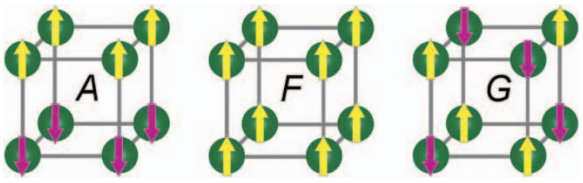

Fig. 4 Schematic illustration of A-type antiferromagnetic, ferromagnetic, and G-type antiferromagnetic structures. The yellow and purple arrows denote the up and down magnetic moments, respectively. Reprinted with permission from Ref. [33].

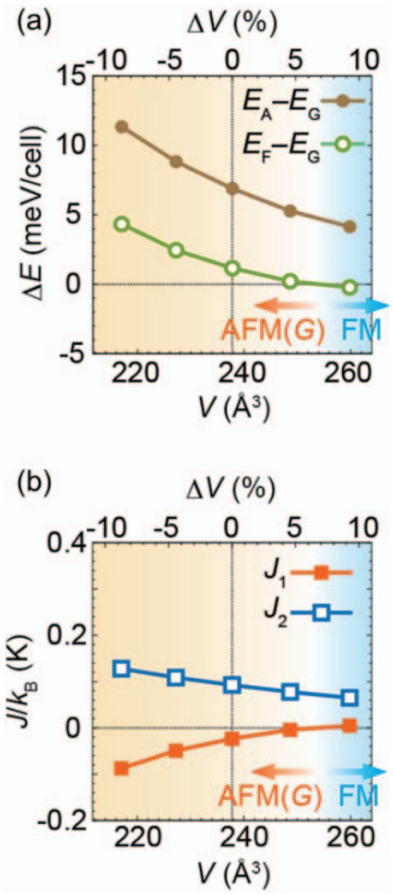

Fig. 5 Lattice volume (V) dependence of (a) energy difference between magnetic structures and (b) exchange coupling constants J_1 and J_2. AFM and FM denote the antiferromagnetic and the ferromagnetic structures, respectively. Reprinted with permission from Ref. [33].

in the lattice volume is zero, i.e., when $EuTiO_3$ is in the stable phase with a cubic perovskite structure, both E_A–E_G and E_F–E_G are positive, indicating that the G-type antiferromagnetic structure is the most stable among the three types of magnetic structures illustrated in Fig. 4. The obtained calculation results conform with the experimental fact that the stable phase of $EuTiO_3$ adopts the G-type antiferromagnetic structure below ~5 K. Furthermore, Fig. 5 (a) indicates that the energy difference between ferromagnetic and G-type antiferromagnetic structures, i.e.,

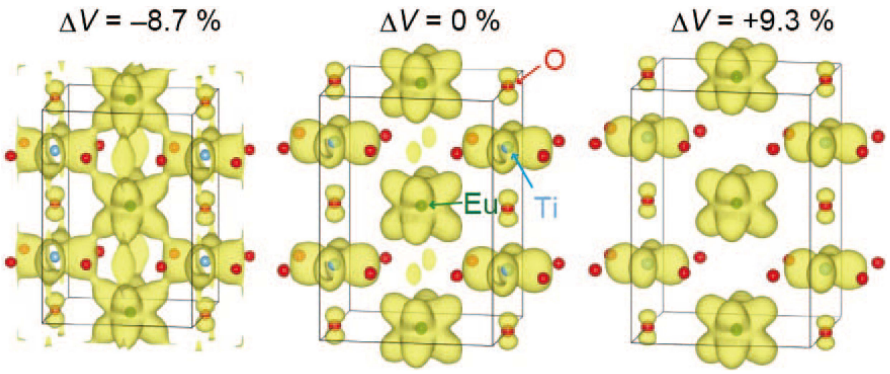

Fig. 6 Change of the charge-density isosurfaces around Eu, Ti, and O with the lattice volume of G-type antiferromagnetic $EuTiO_3$. The change in the lattice volume is denoted by ΔV. Reprinted with permission from Ref. [33].

E_F–E_A, monotonically decreases with an increase in the lattice volume and changes its sign from positive to negative when the increase in the lattice volume exceeds ~5%, indicating that the ferromagnetic structure becomes more stable than the G-type antiferromagnetic structure in the expanded lattice. Figure 5 (b) shows the lattice volume dependence of exchange coupling constants J_1 and J_2. As shown, J_1 monotonically increases with an increase in the lattice volume, and its sign changes from negative to positive when the lattice volume increases beyond ~5%. The change in the energy difference between ferromagnetic and G-type antiferromagnetic structures as well as the variation in the exchange coupling constant between the nearest-neighboring magnetic moments coincide with the experimental result that the magnetization at low temperatures increases with an increase in the lattice volume of the $EuTiO_3$ thin film.

Figure 6 illustrates the charge-density isosurfaces around the Eu, Ti, and O derived by the calculations of G-type antiferromagnetic $EuTiO_3$. The yellowish-green parts correspond to the Eu 4f, Ti 3d, and O 2p orbitals. The overlap between the Eu 4f and Ti 3d orbitals is evident when the lattice is compressed, while such an overlap is not observed when the lattice is expanded. This result suggests that the vacant 3d orbital of Ti^{4+} mediates the negative superexchange interaction between nearest-neighboring Eu^{2+} ions [33]. Furthermore, the ferromagnetic interaction is known to operate between the nearest-neighboring Eu^{2+} ions through the indirect exchange mechanism. In this mechanism, the excitation of 4f spin into the 5d state in an Eu^{2+} ion takes place, subsequently transferring the spin to the 5d state of another Eu^{2+} ion; in addition, the mechanism displays ferromagnetic coupling between the 5d and 4f spins due to the Hund's rule [34]. Consequently, all the 4f spins of the nearest-neighboring Eu^{2+} ions face the same direction. The mechanism is schematically illustrated in Fig. 7. The ferromagnetic and the above-mentioned antiferromagnetic interactions are believed to compete with each other; hence, the stable magnetic structure of $EuTiO_3$ depends on the lattice volume.

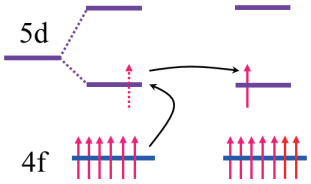

Fig. 7 Schematic of indirect exchange interaction between nearest-neighboring Eu^{2+} ions. The 4f spins are ferromagnetically coupled through the excitation of 4f spin into the 5d level.

Similar calculations based on the density functional theory were performed for $EuZrO_3$, $EuHfO_3$, and $EuSiO_3$ with a perovskite structure [35], although $EuSiO_3$, which adopts the perovskite structure, has never been synthesized. According to the calculations, $EuZrO_3$ and $EuHfO_3$ exhibit a tendency similar to that of $EuTiO_3$. In other words, an expansion of the lattice volume further stabilizes the ferromagnetic structure. In contrast, for $EuSiO_3$, a decrease in the lattice volume stabilizes the ferromagnetic structure. This tendency contrasts those observed for $EuTiO_3$, $EuZrO_3$, and $EuHfO_3$. Such a difference stems from the fact that the antiferromagnetic interaction between Eu^{2+} ions through the Si 3d orbital is not dominant because the energy levels of Eu 4f and Si 3d differ considerably, and the overlap between those orbitals is not very significant. Furthermore, the calculations predict that cubic perovskite-structured $EuZrO_3$ and $EuHfO_3$ should show ferromagnetic transition at low temperatures because the overlap between Eu 4f and Zr 4d/Hf 5d orbitals is large in the orthorhombic structure but lesser in the cubic structure owing to the tilt and rotation of ZrO_6 or HfO_6 octahedra in the orthorhombic structure. Thus, the metastable phases of perovskite-type $EuZrO_3$, $EuHfO_3$, and $EuSiO_3$ display ferromagnetism, while the stable phase of $EuZrO_3$ and $EuHfO_3$ display antiferromagnetism. Nonetheless, the ferromagnetism of these compounds has not yet been experimentally demonstrated. Thus, further studies are required to confirm this theoretical prediction.

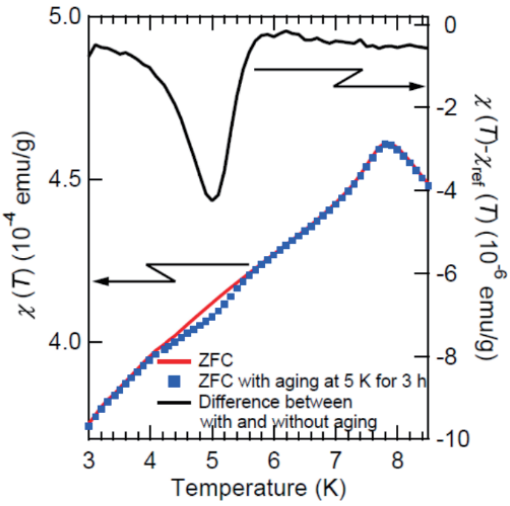

Fig. 8 Temperature dependence of zero-field-cooled magnetic susceptibility for iron phosphate glass with a composition of $30Fe_2O_3 \cdot 15FeO \cdot 55P_2O_5$ in molar ratio. Aging-memory effect is observed.

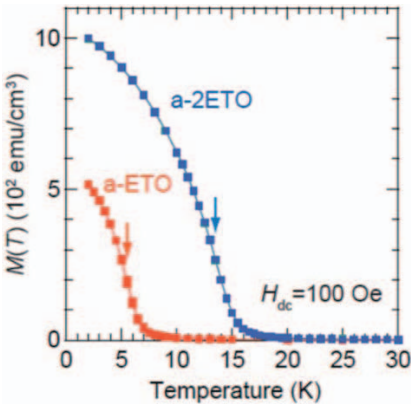

Fig. 9 Temperature dependence of magnetization for amorphous thin films of $EuTiO_3$ (a-ETO) and Eu_2TiO_4 (a-2ETO). The arrows represent an inflection point which corresponds to the Curie temperature. Reprinted with permission from Ref. [49].

4. Ferromagnetism of Amorphous Oxides Containing a Large Amount of Eu^{2+} Ions

The magnetism of amorphous insulators, such as oxide and fluoride glasses, has been examined thus far. Most of these insulators exhibit spin glass transition due to the magnetic frustration, which inevitably occurs in these glass materials because of the randomly distributed magnetic moments in the disordered structure of glass. In addition, the antiferromagnetic interaction is dominant between the nearest-neighboring magnetic moments [36–46]. For example, Fig. 8 shows the zero-field-cooled magnetic susceptibility for iron phosphate glass with a composition of $30Fe_2O_3 \cdot 15FeO \cdot 55P_2O_5$ in mol% [45]. The curve plotted with squares represents the result of aging; the glass sample was kept at 5 K for 3 h without external magnetic field during the cooling process. Evidently, the aging reduced the magnetic susceptibility at 5 K than the simple zero-field cooling process. This result unambiguously indicates that the magnetic phase below the transition temperature, i.e., 7. 8 K, at which the maximum magnetic susceptibility is observed, represents the spin glass.

In contrast to the experimental result that the dominant magnetic interaction between transition metal ions in oxide and fluoride glasses is antiferromagnetic, ferromagnetic interaction was suggested by Schoenes *et al.* [47] for Eu^{2+} ions in amorphous silicate with a composition of $Eu^{2+}_{0.12}Eu^{3+}_{0.02}Si_{0.31}O_{0.55}$ (mol%). They revealed that the Weiss temperature is positive, although it is as low as 1 K. Nonetheless, the ferromagnetic transition was not observed above at least 1.5 K. Akamatsu *et al.* [48] were the first to observe an obvious ferromagnetic transition in amorphous oxides. Based on the temperature dependence of ac magnetic susceptibility of the $60.0EuO \cdot 11.0Al_2O_3 \cdot 19.5B_2O_3 \cdot 9.5SiO_2$ (mol%) glass at varied magnetic fields and ac frequencies, Akamatsu *et al.* [48] clarified that the glass undergoes paramagnetic-to-ferromagnetic transition at 2.2 K. In addition, they determined that the glass exhibits reentrant spin glass behavior. The ferromagnetic transition was also observed for amorphous $EuTiO_3$ and Eu_2TiO_4 thin films deposited on a silica glass substrate through the PLD method [49]. Figure 9 shows variation in magnetization with respect to temperature (M–T curve) for amorphous $EuTiO_3$ and Eu_2TiO_4, which are represented by a-ETO and a-2ETO, respectively. The M–T curves for both amorphous oxides characterize a ferromagnetic material, and the Curie temperature evaluated from the inflection point (indicated by arrows; Fig. 9) is 5.5 and 14 K for amorphous $EuTiO_3$ and Eu_2TiO_4, respectively. Thus, amorphous $EuTiO_3$ undergoes ferromagnetic transition at 5.5 K in contrast to the fact that the stable phase of crystalline $EuTiO_3$ becomes antiferromagnetic below 5.3 K [24]. The magnetic moments originating from the Eu^{2+} ions face the same direction in amorphous $EuTiO_3$ irrespective of the random distribution of magnetic moments peculiar to the amorphous structure. Furthermore, both crystalline and amorphous Eu_2TiO_4 are ferromagnetic, and interestingly, the Curie temperature of the amorphous phase is rather higher than that of the crystalline phase (9 K) [34], which is considered a rare phenomenon. Usually, the magnetic-phase transition temperature is reduced by approximately one order of magnitude when a crystalline material is converted into its amorphous phase with a constant composition. Some examples are listed in Table 1 [50–55].

To disclose the origin of the ferromagnetism observed for amorphous $EuTiO_3$ and Eu_2TiO_4, the local structure around the Eu^{2+} ion was examined using the extended X-ray absorption fine-structure spectroscopy [56]. The results indicate that the oxygen coordination number (CN)

Table 1 Magnetic ordering and phase transition temperature of some crystalline and amorphous compounds based on iron oxide.

Compound		Magnetic ordering	Transition temperature (K)	Ref.
Fe_2O_3	Crystalline	Weak ferromagnetic	950	50
	Amorphous	Cluster spin glass	35.1±0.1	51
$Y_3Fe_5O_{12}$	Crystalline	Ferrimagnetic	560	52
	Amorphous	Diluted antiferromagnetic	40	53
$BiFeO_3$	Crystalline	Antiferromagnetic	643	54
	Amorphous	Spin glass	20	55

for Eu^{2+} differs between the crystalline and amorphous phases. That is, CN = 12 and 9 for crystalline $EuTiO_3$ and Eu_2TiO_4, respectively, while CN = 6 for both amorphous $EuTiO_3$ and Eu_2TiO_4. In other words, the crystal-field strength, which causes the splitting of the 5d level, as illustrated in Fig. 7, is more intense for amorphous phases than for crystalline phases. Hence, for the amorphous phases, the excitation of the 4f spin into the lowest 5d level occurs easily, resulting in the ferromagnetic coupling between the nearest-neighboring Eu^{2+} 4f spins (see Fig. 7). The X-ray magnetic circular dichroism at the Eu $M_{4,5}$ and $L_{2,3}$ edges was measured at various temperatures for amorphous $EuTiO_3$ and Eu_2TiO_4 [57]. The results clearly indicate magnetic polarization of both 4f and 5d states, demonstrating that the 4f–5d indirect exchange interaction is the essential factor displaying the ferromagnetism in amorphous $EuTiO_3$ and Eu_2TiO_4. In addition, these amorphous phases exhibit the Faraday effect in the visible range and possess a Faraday rotation angle comparable to that of crystalline EuSe [58], a magnetic semiconductor. Here, note that magnetic semiconductors, such as EuO, EuS, EuSe, and (Cd,Hg,Mn)Te, are known to display a large Faraday effect in the visible range, some of which have been practically utilized in a device such as an optical isolator [59]. Therefore, the amorphous oxides analyzed in this study are a promising candidate for use in optical isolators in the visible region.

5. Summary

The metastable phase of some oxide materials possesses a magnetic functionality superior to its stable counterpart. In this study, it is shown that $ZnFe_2O_4$ with a spinel-type structure becomes ferrimagnetic with high magnetization and a phase-transition temperature higher than room temperature when its metastable structure, with random cation distribution, is achieved. The superexchange interaction between Fe^{3+} ions at the tetrahedral and octahedral sites is the origin for the ferrimagnetism. In addition, ferromagnetic state is stabilized further in $EuTiO_3$ with a perovskite-type structure, with an increase in the lattice volume, while the stable phase of $EuTiO_3$ undergoes antiferromagnetic transition. This is because the increase in lattice volume suppresses the antiferromagnetic interaction between Eu^{2+} ions based on the vacant 3d orbital of Ti^{4+}, as suggested by the first-principles calculations. The theoretical calculations also predict that the cubic phases of $EuZrO_3$ and $EuHfO_3$, the stable phases of which are orthorhombic, should be ferromagnetic. Furthermore, amorphous oxides bearing a large amount of Eu^{2+} ions, including the amorphous thin films of the EuO-TiO_2 system, exhibit ferromagnetic transition. It is believed that the large splitting of the 5d level of Eu^{2+} in amorphous EuO-TiO_2 system results in the overcoming of the antiferromagnetic interaction by the ferromagnetic interaction based on the indirect exchange mechanism.

Acknowledgment

The author would like to thank the following members for their great contributions to this research: Prof. Koji Fujita, Dr. Seisuke Nakashima, Prof. Kazuyuki Hirao, Dr. Hirofumi Akamatsu, Prof. Isao Tanaka, Dr. Tomoyuki Yamamoto, Dr. Shunsuke Murai, Dr. Yanhua Zong, Mr. Naoki Wakasugi, Mr. Yuya Maruyama, Dr. Naohiro Takemoto, Dr. Takahiro Kawamoto, Dr. Yoshiro Kususe, Prof. Fumiyasu Oba, Dr. Yu Kumagai, and Dr. Hiroyuki Hayashi of Kyoto University and Dr. Tetsuya Nakamura, Dr. Toyohiko Kinoshita, Dr. Masaichiro Mizumaki, Dr. Naomi Kawamura, and Dr. Motohiro Suzuki of Japan Synchrotron Radiation Research Institute, SPring-8.

[1] S. Chikazumi, *Physics of Ferromagnetism*, Vol. II (Shokabo, Tokyo, 1984) [in Japanese].
[2] M. Taguchi *et al.*, Phys. Rev. Lett. **115**, 256405 (2015).
[3] Y. Kajiwara *et al.*, Nature **464**, 262 (2010).
[4] J. Matsuno *et al.*, Sci. Adv. **2**, e1600304 (2016).
[5] Y. Onose *et al.*, Science **329**, 297 (2010).
[6] T. Kimura *et al.*, Nature **426**, 55 (2003).
[7] D. Vaknin *et al.*, Phys. Rev. Lett. **92**, 207201 (2004).
[8] Y. Yamasaki *et al.*, Phys. Rev. Lett. **96**, 207204 (2006).

[9] T.S. Boescke *et al.*, Appl. Phys. Lett. **99**, 102903 (2011).
[10] M. Kobayashi *et al.*, IEEE J. Electron Dev. Soc. **6**, 280 (2018).
[11] E.F. Westrum and D.M. Grimes, J. Phys. Chem. Solids **3**, 44 (1957).
[12] C.M. Srivastava *et al.*, Bull. Mater. Sci. **6**, 27 (1984).
[13] K. Tanaka *et al.*, J. Magn. Magn. Mater. **131**, 120 (1994).
[14] K. Tanaka *et al.*, J. Phys. Chem. Solids **59**, 1611 (1998).
[15] K. Tanaka *et al.*, J. Phys.: Condens. Matter **15**, L469 (2003).
[16] S. Nakashima *et al.*, J. Phys.: Condens. Matter **17**, 137 (2005).
[17] S. Nakashima *et al.*, Phys. Rev. B **75**, 174443 (2007).
[18] K. Tanaka *et al.*, J. Appl. Phys. **99**, 106103 (2006).
[19] S. Nakashima *et al.*, J. Ceram. Soc. Jpn., Supplement **112**, S961 (2004).
[20] S. Nakashima *et al.*, J. Magn. Magn. Mater. **310**, 2543 (2007).
[21] N. F. Borrelli and J. A. Murphy, J. Appl. Phys. **42**, 1120 (1971).
[22] H. Takeuchi, Jpn. J. Appl. Phys. **14**, 1903 (1975).
[23] S. Wittekoek *et al.*, Phys. Rev. B **12**, 2777 (1975).
[24] T. Katsufuji and H. Takagi, Phys. Rev. B **64**, 054415 (2001).
[25] T. Kolodiazhnyi *et al.*, Appl. Phys. Lett. **96**, 252901 (2010).
[26] Y. Zong *et al.*, J. Solid State Chem. **183**, 168 (2010).
[27] H. Akamatsu *et al.*, Inorg. Chem. **51**, 4560 (2012).
[28] C.J. Fennie and K.M. Rabe, Phys. Rev. Lett. **97**, 267602 (2006).
[29] R. Ranjan *et al.*, J. Phys.: Condens. Matter **19**, 406217 (2007).
[30] K. Fujita *et al.*, Appl. Phys. Lett. **94**, 062512 (2009).
[31] J.H. Lee *et al.*, Nature **466**, 954 (2010).
[32] K. Tanaka *et al.*, J. Mater. Res. **28**, 1031 (2013).
[33] H. Akamatsu *et al.*, Phys. Rev. B **83**, 214421 (2011).
[34] C.L. Chien *et al.*, Phys. Rev. B **10**, 3913 (1974).
[35] H. Akamatsu *et al.*, Adv. Funct. Mater. **23**, 1864 (2013).
[36] A. Verhelst *et al.*, Phys. Rev. B **11**, 4427 (1975).
[37] H.R. Rechenberg *et al.*, J. Appl. Phys. **49**, 1638 (1978).
[38] J.P. Renard *et al.*, Solid State Commun. **35**, 41 (1980).
[39] J.P. Sanchez *et al.*, J. Phys. C **17**, 127 (1984).
[40] J.P. Sanchez and J.M. Friedt, J. Phys. (Paris) **43**, 1707 (1982).
[41] J.L. Shaw *et al.*, J. Non-Cryst. Solids **345**, 245 (2004).
[42] H. Akamatsu *et al.*, Phys. Rev. B **74**, 012411 (2006).
[43] H. Akamatsu *et al.*, J. Magn. Magn. Mater. **310**, 1506 (2007).
[44] H. Akamatsu *et al.*, J. Phys.: Condens. Matter **20**, 235216 (2008).
[45] H. Akamatsu *et al.*, Phys. Rev. B **80**, 134408 (2009).
[46] H. Akamatsu *et al.*, Phys. Rev. B **84**, 144408 (2011).
[47] J. Schoenes *et al.*, Phys. Status Solidi A **51**, 173 (1979).
[48] H. Akamatsu *et al.*, Phys. Rev. B **81**, 014423 (2010).
[49] H. Akamatsu *et al.*, Phys. Rev. B **82**, 224403 (2010).
[50] L. Néel, Ann. Physik **3**, 137 (1948); **4**, 249 (1949).
[51] M.D. Mukadam *et al.*, Phys. Rev. B **72**, 174408 (2005).
[52] R. Pauthenet, J. Appl. Phys. **29**, 253 (1958).
[53] E.M. Gyorgy *et al.*, J. Appl. Phys. **50**, 2883 (1979).
[54] J. Moreau *et al.*, J. Phys. Chem. Solids **32**, 1315 (1971).
[55] S. Nakamura *et al.*, J. Appl. Phys. **74**, 5652 (1993).
[56] Y. Zong *et al.*, J. Am. Ceram. Soc. **95**, 716 (2012).
[57] T. Kawamoto *et al.*, Phys. Rev. B **88**, 024405 (2013).
[58] J.C. Suits and B.E. Argyle, J. Appl. Phys. **36**, 1251 (1965).
[59] K. Onodera *et al.*, Electron. Lett. **30**, 1954 (1994).